Seismic Catalog Analysis & Quality Verification for the Geysers Geothermal Field, California

by

Austin Abreu

Department of Earth Sciences, University of California Santa Cruz

ERTH 191C: Practical Geophysics

Dr. Ricardo Garza-Giron

March 16, 2022

1 Purpose & Scope

As the Geysers Geothermal Field ("The Geysers") aims to implement Enhanced Geothermal technology, it becomes necessary to identify key sites for implementation. Similarly, as seismic localities fluctuate throughout the field, seismic analysis will aid in predicting changes in structure and pressure demand within the geothermal field. Characterizing the location, mechanisms, and distribution of seismic activity in the area is paramount to the exploitation of the valuable dry-steam resource as well as advancement of scientific understanding of geothermal systems. This project aims to temporally and spatially relate seismic events in the context of the geothermal exploitation occurring in the field area, as well as verify the integrity of the existing NCEDC catalog. We utilized graphical analysis to identify features in the seismic catalog, and thus the geothermal field, to inform magnitude analysis. Magnitude analysis was carried out using the Gutenberg-Richter relation to test for completeness, and graphical analysis was used to isolate seismic zones. Finally, catalog quality control was performed by analyzing the catalog with a neural network and performing stand-alone location analysis.

2 Introduction

2.1 Geologic Setting

The Geysers lie at the southern edge of the Clear Lake Volcanic Complex (CLV), an active volcanic system approximately 2.1 Ma in age (Hearn, Donnelly-Nolan, and Goff, 1995; Dalrymple et al., 1999;), making it the youngest and northernmost of a series of volcanic centers extending to the southeast. The region lies along the boundary of the North American plate, tectonically controlled by the Mendocino Triple Junction to the north and San Andreas Fault to the west (Johnson & O'Neil, 1984). Clear Lake volcanism is believed to be the consequence of a slab-free window that developed following the northward translation of the Triple Point through the region, and subsequent transition from subduction to transform fault regimes. (Peacock et al., 2020, & references therein). The Clear Lake volcanics overlay the Franciscan assemblage of Jurrassic to Eocene age; the Great Valley Sequence of Jurassic to Cretaceous age; and various sedimentary deposits of Paleocene to Eocene age. Active volcanism occurred concurrently with sedimentary deposition in the Pliocene to Pleistocene, which is formally grouped as the Cache Formation. Due to heavy deformation within the Tertiary to late Quaternary, the Great Valley sequence is detached and emplaced above Franciscan rocks northeast of the Geysers, and Franciscan units are imbricated within Coast Range Ophiolite members within the Geysers. The Clear Lake area as a whole lies stratigraphically above Coast Range Ophiolite, which is an accretionary complex composed of mafic & ultramafic metavolcanic facies. (Donnelly et al., 1977; McLaughlin, 1981).

Local to The Geysers, the Franciscan Assemblage is surficially uplifted and overlain with the Cobb Mountain rhyodacite (Hearn et. al, 1995). The Franciscan assemblage is a variably metamorphosed meta-sedimentary complex that includes sandstone, chert, conglomerate, minor limestones, and argillite, as well as pillow basalts and meta-volcanics such as greenstone, blueschist, serpentinite, amphibolite, and eclogite. These rocks are structurally apparent through reactivated thrust faults and appear in character ranging from coherent bedding to melange. Melange portions are typified by dominance of metavolcanics (Donnelly et al., 1977; McLaughlin, 1981).

Embedded within the Franciscan Assemblage is an average age 1.33 ± 0.04 Ma (Schmitt et al., 2003a) felsic pluton-scale body composed of three distinguishable rock types: 1.46 ± 0.03 & 1.16 ± 0.02 Ma biotite- orthopyroxene granite, 1.75 ± 0.01 Ma biotite pyroxene(?) microgranite porphyry, and 1.27 ± 0.01 Ma hornblende-biotite-orthopyroxene granodiorite. (Hulen & Nielson, 1996; Schmitt et al., 2003b). Dalrymple et. al. (1999) Schmitt et. al. (2003b) believe the Geysers Plutonic Complex (GPC) to be indistinguishable in age from Cobb Mountain rhyodacites under Zircon U-Pb inspection. The granite forms the base of the pluton beginning below -1219 m, with the microgranite forming the "core" of the pluton. The granodiorite is coincident

Figure 1

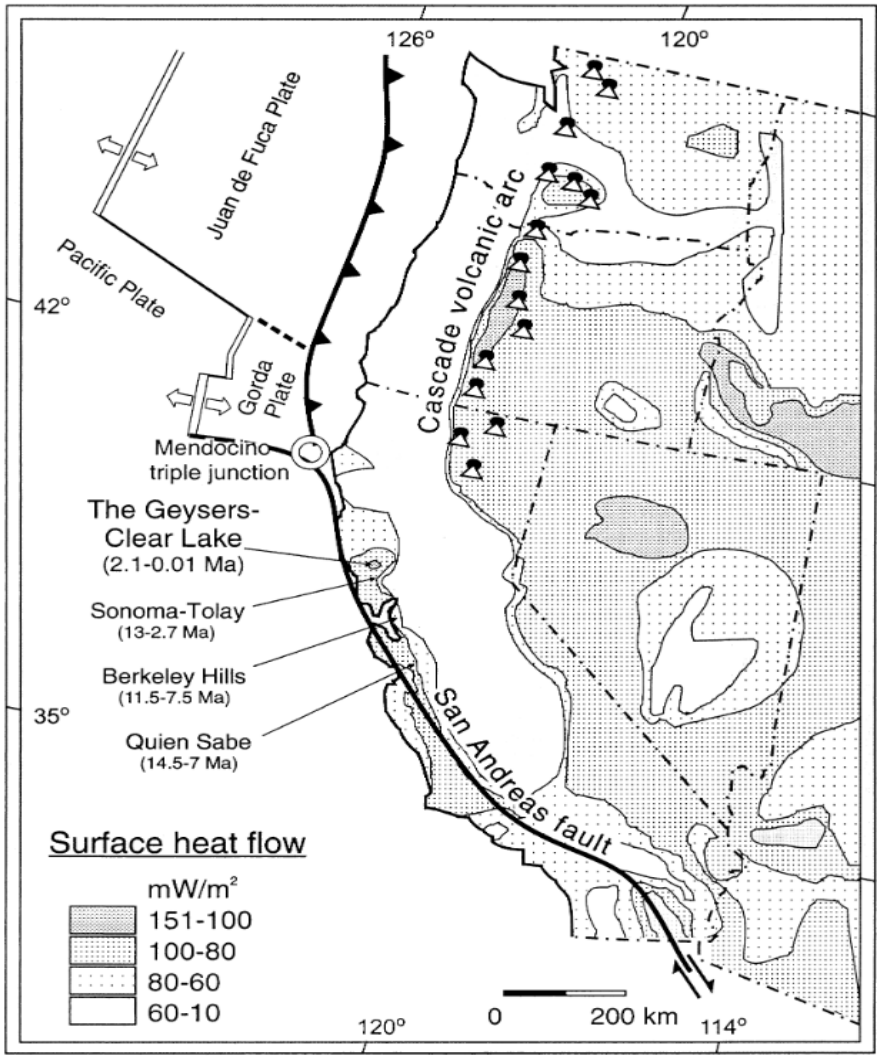

Map of the regional tectonics and heat flow showing the location of the field area relative to plate boundaries, including the location and age of sibling volcanic centers along the plate margin.
Reprinted from Schmitt, A. K., Grove, M., Harrison, T., Lovera, O., Hulen, J., & Walters, M. (2003b). The Geysers-Cobb mountain magma system, california (part 2): Timescales of pluton emplacement and implications for its thermal history. Geochimica et Cosmochimica Acta, 67(18), 3443–3458. https://doi.org/10.1016/s0016-7037(03)00126-1

with the granite, but occurs only in the southeastern portion of the field area (Hulen & Nielson, 1996).

The development of the geothermal reservoir began 1.2 million years ago, but was fluid-dominated until as recently as 0.3 m.y.a. Subsequent boiling, then repressurization of phreatomagmatic fluids led to the formation of the modern vapor-dominated reservoir. The reservoir follows the contour of the GPC at depth, but lies within the Franciscan assemblage above the pluton.The steam reservoir extends to a depth of approximately 2.5 km and maintains a temperature of approximately 240°C in the northwest (NW) and southeast (SE) region of the geothermal field (Johnson et al., 2016). The NW region contains a high-temperature zone that rests between 2.5 km and 4 km depth; temperatures in this zone reach 400°C. (Peacock et al., 2020 & references therein).

2.2 Tectonic Setting

The Clear Lake area rests atop the eastern edge of the San Andreas Fault (SAF) Zone, with the Collayomi Fault zone (trending northwest) and the Konocti Bay fault zone (trending north-northwest) representing the primary fingers of the SAF zone in the area (McLaughlin, 1981,). It has been shown by Boyle & Zoback (2014) that local maximum horizontal stress is oriented parallel to the NNE-SSW trending regional stress field. However, local faulting follows extensional and oblique strike-slip regimes that contradict the regional fault regime. (Yu et al., 2018). According to Leptokaropoulos et al. (2018) & references therein, the tectonic stress in the area has little effect on seismic activity relative to the changing pore pressure in The Geysers.

Consequently, seismicity in the geothermal field is exemplified by small, shallow events produced by a large number of short, diversely oriented faults. As early as Bufe, et al. (1981), the seismic activity is described as largely induced on account of the area's high b-values, temporal distributions of fault-plane solutions within the geothermal field, and nearly continuous occurrence of seismic events. Since Bufe et. al, contemporaneous sources have quantified the proportional increase in seismicity rate at The Geysers following effluent injection (Majer, et al., 2007; Leptokaropoulos, 2020 & references therein).

Majer et al. (2007) reports a time lag of < 2 months for deep-injection-induced seismicity, which is corroborated in The Geysers by Johnson et al. (2016) and Leptokaropoulos et al. (2017) to a window as early as 2 weeks and as late as 6 months. Event hypocenters are correlated with fluid movement through the reservoir, in particular below the average depth of injection (> 2km) on account of gravitational drawdown, with events distal from the injection site occurring later in time. Leptokaropoulos et al. (2017) identified strong correlation between injection rate and changes in b-value local to the injection site. While Leptokaropoulos (2020) found the magnitude distribution does not follow the GR, that study used a modified catalog (originally sourced from the NCEDC), and utilized statistical analysis methods that are outside the scope of this project. Statistical seismology methods used by Johnson et al. (2016) are consistent with the methods used in this study, and will be used as a point of reference.

3 Data & Methods

The Northern California Earthquake Data Center (NCEDC) has managed the seismic network surrounding the geothermal field since 1991; in 2003 the Lawrence Berkeley National Laboratory (LBL) initiated an array of 31 500 Hz stations within the geothermal field. The NCEDC operates a variety of networks, with stations relevant to this survey being in the 100 Hz NC network. Catalog data for both networks was downloaded from the NCEDC repository between the years 2003 and 2016 (https://service.ncedc.org/, accessed March 5, 2022), within the geographic region bounded by the 38.7 & 39.5 latitudes and -122.90 & -122.65 longitudes. This region is slightly larger than The Geysers proper. Within the study period, the LBL catalog contains 317,187 $M_L \geq 0$ events; the NCEDC catalog contains 172,991 events. This difference is accounted for by each network's density of stations relative to the geothermal field, the methods each network uses to identify events, and the response rate of the stations in each network. For both networks event hypocenters are calculated using standard single-event location techniques described by Thurber (1981), utilizing a velocity structure that is annually adjusted (Guilhem et al., 2014, Hutchings et. al, 2014; Johnson et. al, 2016). Magnitudes are computed using the duration coda method in the NCEDC catalog, while the LBNL catalog uses a local magnitude scale. Neither equation is known for these providers. Events within these catalogs were not correlated using mathematical or statistical methods. Instead, we aim to evaluate the similarities between the catalogs using a number of analytical methods, described in the following sections.

The Geysers may be divided in a northwestern and southeastern region, analogous to the Cobb Creek lineament from Hulen and Nielson (1996), on account of seismicity rates, reservoir characteristics, and seismic station configuration. Following regional analysis of each parameter, the field area was divided into NW and SE regions and the regions were analyzed using the same methods to identify differentiating characteristics. The NW region contains 75% of the events in the LBNL catalog, and 76% of events in the NCEDC catalog,

Figure 2

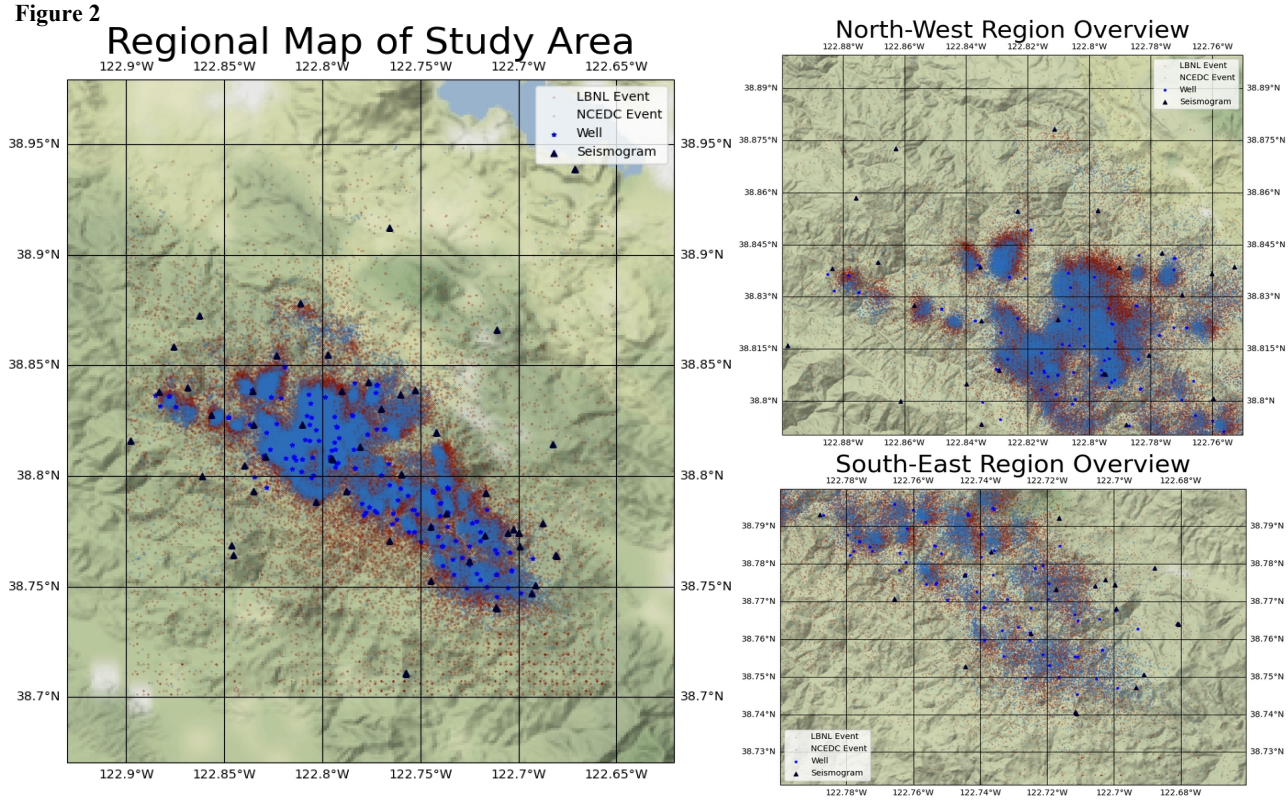

Geographic view of the study area with seismic events, injection wells, and seismograms plotted. Blue represents NCEDC events; red represents LBNL events. These colors are consistent throughout the paper.

3.1 Temporal Analysis

The seismic catalog was temporally analyzed by generating cross-sections in time with respect to latitude, longitude, and depth to identify temporally distinct events within the geothermal field. A depth histogram allowed us to isolate the seismic zone in the subsurface, and a magnitude histogram was used to determine the magnitude of completeness. Quarter-year windows were used to study changes in frequency across the year. C. W. Johnson et al. (2016) describe seasonal fluctuations in seismicity proportional to changes in effluent injection volume, with a time-delay of ≤ 6 months, verification of which will validate the catalog.

3.2 Spatial Analysis

Spatial analysis was conducted using latitude-longitude plots to characterize the map-view locale of seismic activity, then cross-referenced with cross sections along latitude and longitude. Magnitude distributions at depth were employed following these steps to identify structures or seismic zones and infer their nature. Due to the relationship between well location and seismic activity, well locations were used to spatially organize events.

3.3 Magnitude Analysis & Statistics

Each catalog underwent magnitude analysis to test regional adherence to the Gutenberg-Richter (GR) law. Each catalog was first subjected to maximum curvature analysis as described by Wiemer and Wyss (2000) to identify the catalog's magnitude of completeness (M_C), which was employed to perform the maximum likelihood estimation of the b-value described by Aki (1965). This method utilizes linear regression techniques to quantify the linearized frequency of magnitude distributions, the b-value. The b-value is then taken to develop causal correlations for the observed magnitude distribution (El-Isa & Eaton, 2014). Following

this method, catalog entries below the magnitude of completeness were removed from analysis, in order to ensure statistical integrity.

In addition, observations from spatial and temporal analysis were utilized to develop granular analyses of magnitude distributions. Events were correlated with well locations, and eccentricities in data were analyzed for novelty.

3.4 Quality Control

Each catalog was tested against an independently generated catalog for a duration of one weeks' worth of time series data. The number of events detected in each week by the catalogs was accumulated, and weeks with less than 300 events were filtered out. We elected to analyze the window between 22-2-2015 & 27-2-2015 because it had approximately 300 events, and we infer from the recency of the time window higher quality data across all catalogs and seismograms.

The test catalog was generated by EQTransformer (EQT), a neural network developed by Mousavi et al. (2020). The network input parameters were set to 0.1 for all thresholds, and picks were analyzed individually for robustness following generation. The picks were then associated using the built-in association function. The origin times for each event in the EQT catalog were then compared against each pick in the LBNL and NCEDC catalogs using a time-difference method with a tested range of 3 seconds. Finally, hypocenter locations were calculated with the EQT picks using a S-P delay method, where:

$$d = \frac{t_s - t_p}{1/v_s - 1/v_p}$$

To generate a distance surrounding the corresponding station. This distance allows one to triangulate the location of an event by determining the intersection of multiple radii. These radii were then plotted alongside the correlated catalog picks to determine accuracy.

To utilize EQT we took care to choose stations that were distributed throughout the study area. While we intended to choose as many NC network stations as possible, we were only able to use one. We downloaded waveform data for BG.[ACR, AL6, DEB, EPR, LCK, PFR, RGP, SQK, TCH] and NC.GAXB from the NCEDC FDSN network through EQT's built-in downloading client. Use of the internal function of EQT is important to its functionality, but these systems utilize existing FDSN lookup paths.

4 Results

4.1 Catalog Analysis

4.1.1 Spatial Analysis

Spatial analysis of the catalogs revealed a clear correlation between well location and event location, as expected based on research by Johnson et al. (2016), Leptokaropoulos et al. (2017), and others. Density of events within the primary exploitation zone is too high to properly correlate with well location without advanced mathematical modeling, which is out of the scope of this paper. However, visual analysis marks clear correlation

both in plan-view and in cross-section. Both catalogs show depth-oriented features that strike along identical lines of latitude and longitude. Cross-referencing these features with well locations mark weak correlation. We instead take these phenomena to relate to structures responsible for seismic events such as fractures or fault planes.

Cross sections of the field along latitude show higher concentrations of events in the northern region of the field, where the density of injection wells is greater, and the HTZ resides. This is consistent with findings from Majer et. al (2014), Peacock et. al (2020), and others. Cross sections along longitude correlate this relationship. Longitudinal cross sections highlight features within the -122.80 to -122.90 longitudes taken to represent the migration of seismicity into the HTZ, which lies at greater depth than the average reservoir depth.

The LBNL catalog captures events at greater depth than the NCDEC catalog, likely due to higher station density and particular frequency response of its instruments. The LBNL catalog has an average depth 1.04 km greater than the NCEDC catalog. Event depths in the NW region are 0.68 km deeper on average compared to the SE region. Event depths in the NW region fall noticeably below the depth of the pluton and show clear distinction in the HTZ. In the SE zone a bimodal

distribution appears, with depths peaking at 0 km depth, and again at just below 2km. The NCEDC does not show the resolution displayed in the LBNL catalog across many depths.

Events within both catalogs show clear spatial correlation, although there is a distinct difference in homogeneity of locations. While both catalogs purport to contain accurate locations, the LBNL catalog appears to use grid-based algorithmic placement for their events, as evidenced by obvious horizontal lineaments in cross-sections and in square-like clusters in map view. This is contrasted by the NCEDC catalog, which appears to have organically organized event locations. Analysis of the two catalogs alongside each other makes a difference in location strategies obvious.

4.1.2 Temporal

Analysis through time in The Geysers showed distinct cycles of seismicity consistent with findings from Johnson et. al (2016) and Majer et. al (2014). In particular, seasonal fluctuations in seismicity–allegedly proportional to increases in injected water volume–are observed only by using simple counting methods. Figure A, on the title page, details the change in seismicity after the turn of the year, often with a delay on the scale of months, followed by decreases in seismicity toward the end of each year.

Translation of seismic zones was not evaluated using the non-rigorous methods in this study. Analyses of latitude and longitude over time did not reveal obvious changes in seismic locale. However, investigation of these relationships revealed a comparison of the catalog event locations. On account of event density and ambiguity of events, this relationship is difficult to see for many sample points in map view. Instead, cross-sections of longitude in time, as seen in Figure X, makes discriminating between the NCEDC and LBNL catalogs easy. We find the NCEDC and LBNL catalog locations to correlate very strongly for correlated events, both in time and space. Mathematical analysis was not performed on account of the strong visual correlation between events across many sample windows. However, a more rigorous analysis would employ fuzzy matching windows to identify correlated events. Instead, we focused those

Figure 4

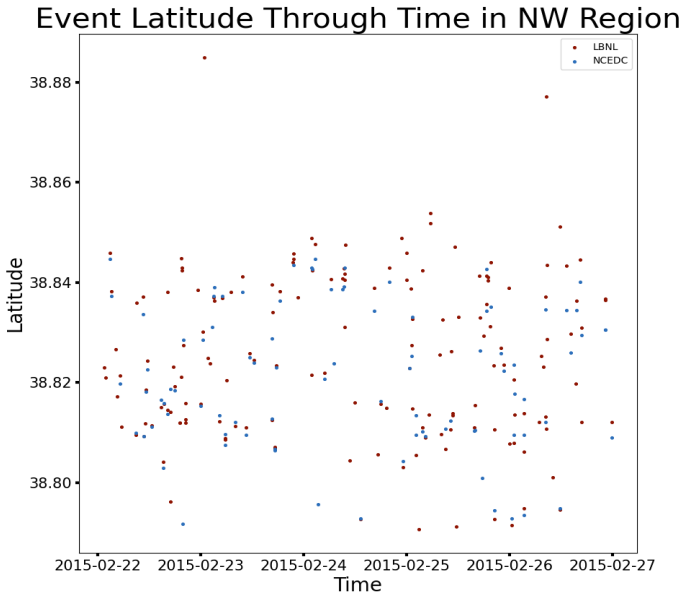

After inspecting each geospatial dimension individually, and with a smaller window of samples, it became clear the LBNL and NCEDC catalogs contained the same temporo-spatial seismic events.

Figure 3

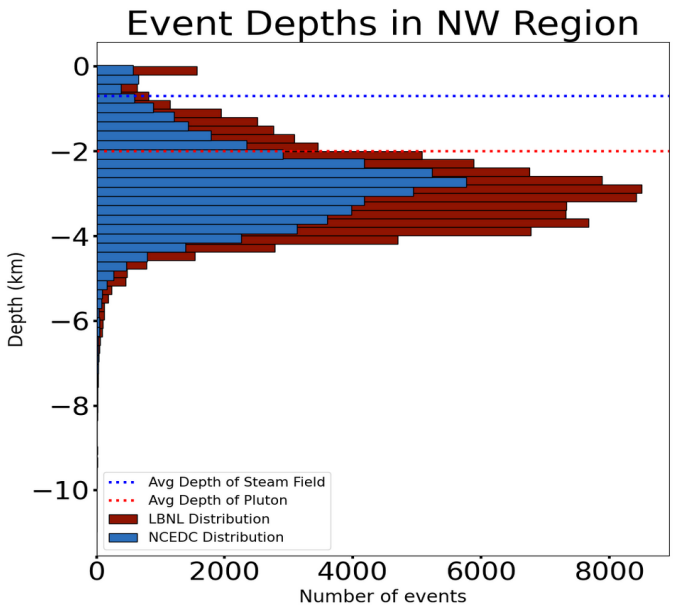

Distribution of event depths in the NW region of the geothermal field. The character of events in this region is higher intensity, and at greater depth, which is corroborated by other research.

Figure 5

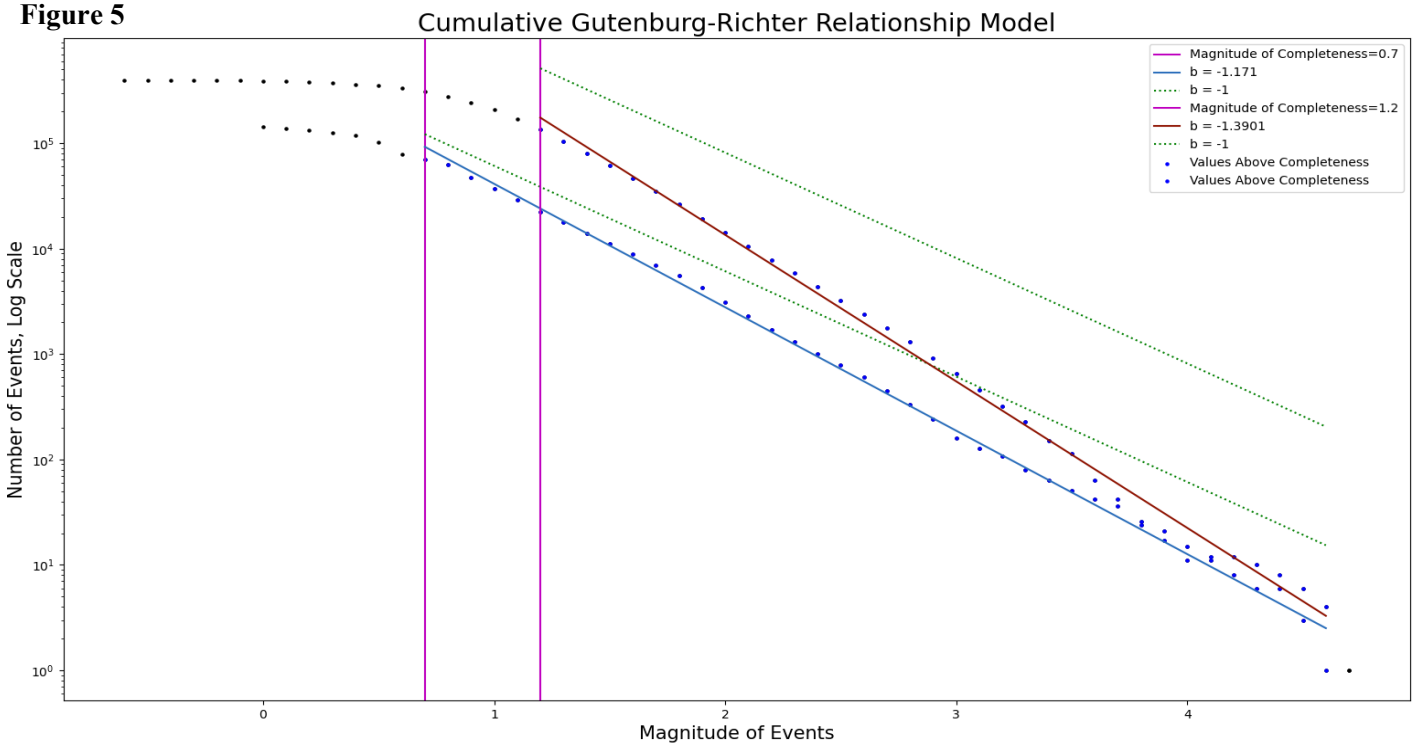

Above, the histogram of event magnitudes for both catalogs. The NCEDC catalog has a strange, uneven distribution, most likely due to the low sensor density in the region. Below, the Gutenburg-Richter model with LBNL b-value in red, NCEDC in blue. Both values are above one, indicating greater frequency of low-intensity earthquakes. Pink lines mark the Magnitude of Completeness for each catalog.

efforts on independently verifying the catalogs as if they were discrete using the methods previously described.

4.1.3 Magnitude

The NCEDC and LBNL catalogs displayed remarkable differences in magnitude distributions. Using the maximum curvature method, the catalogs returned $M_{C,d} = 0.7$ and $M_{C,L} = 1.2$, respectively. Maximum likelihood estimation returned a *b-value = -1.171* for NCEDC, and *b = -1.3901* for LBNL. These values suggest that smaller seismic events are more frequent than large events, matching our prior understanding of seismicity in the geothermal field.

Cross-referencing magnitudes with spatial dimensions or time did not reveal novel information. Inspecting magnitude distributions over latitude or longitude localized higher magnitude events within the core of the geothermal field, which is not surprising. Analysis of magnitude in time weakly correlated events in classic mainshock-aftershock sequencing. Indeed, it is possible this phenomenon does occur in The Geysers, but the proliferation of small amplitude events makes correlations between discrete events difficult.

Magnitude analysis of the NW and SE zones returned statistical values close to the overall regime. In the NW zone, NCED and LBNL catalogs returned maximum curvature estimates of $M_{C,d} = 0.8$ & $M_{C,L} = 1.2$; and $b = -1.1636$ & $b = -1.3663$, respectively. Maximum curvature values were identical in the SE zone, with a -7% change from NCEDC's regional b-value and +1% change in LBNL's b-value. The LBNL's stable b-value across subdivisions is a testament to the robustness of the catalog. The variance in NCEDC's b-values is likely on account of the lack of events in the SE region, and geothermal field as a whole. The SE region's low intensity seismicity could be responsible for its lack of inclusion in the NCEDC catalog.

4.2 Quality Control

Within the time window 22-2-2015 to 27-2-2015, LBNL and NCEDC catalogs contain 310 events combined (201 LBNL events, 109 NCEDC events). Using 10 stations, in the same window of time EQT detected 914 events. Due to the low threshold parameters, it was expected that we would receive a large number of events. However, a difference of 300% was unexpected. In the future–and in particular for The Geysers, where the seismicity rate is very high, events very shallow, and intensities very low–finer tuning of the parameters of EQT will be necessary to accurately identify events.

4.2.1 Pick Quality

Of the 914 events identified by EQT: 200 of these events were correlated to LBNL events, and all NCEDC events were correlated. These events fall within a ±3 second window around the corresponding EQT event, and are phase agnostic (as are both provider catalogs). Of these correlated events, the average time deviation is 1 second for NCEDC, 1.4 for LBNL. Therefore, it's possible to reduce the window; however, our algorithm already checks for and excludes duplicates.

4.2.2 Location Quality

The distance of each event from the receiver stations was algorithmically generated, and 5 of each were plotted schematically along with the corresponding LBNL or NCEDC event. Our results failed to visually correlate with the locations presented by the provider catalogs. We know from previous research that the velocity structures for The Geysers are understood and regularly updated. The difference in our locations, which are calculated using the Wadati-Benioff velocities for S- and P-waves, can be attributed to this as well as more complicated hypocenter calculation methods.

Figure 6

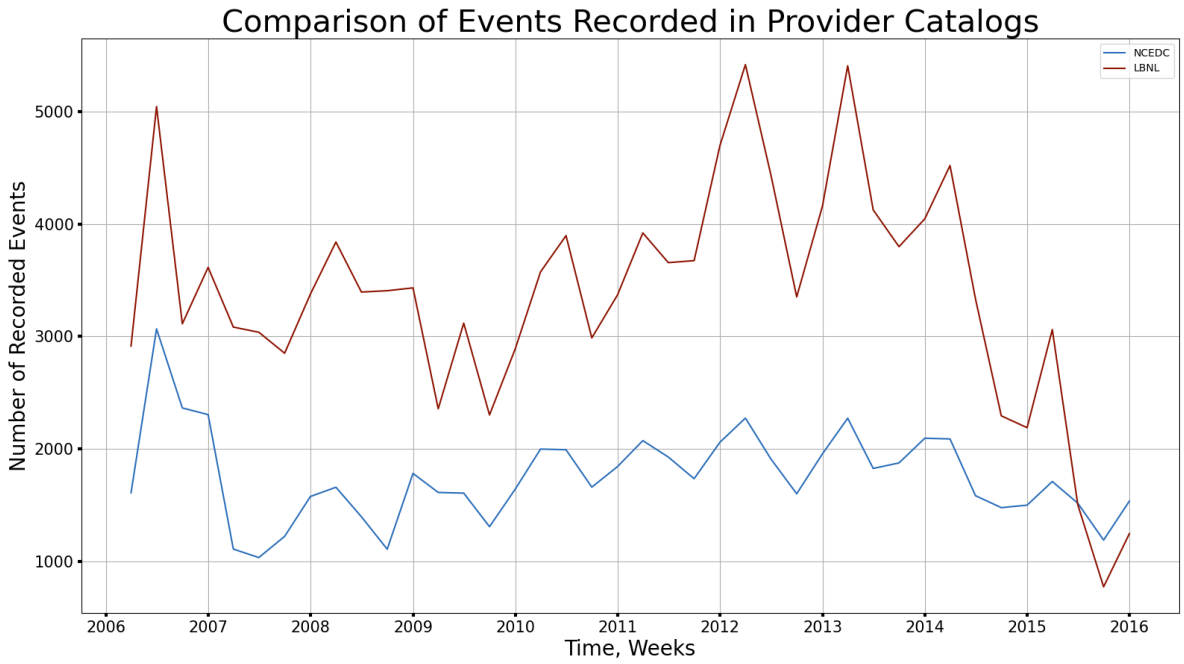

Average events in each quarter over the entire catalog duration. This figure corroborates findings by Johsohn (2016), Majer (2007), and Leptokaropoulos (2020) regarding delay time between injection volume and increases in seismicity rates. Of particular note are the first quarters of each year, where seismic event volume spikes regularly in proportion to increased energy demands in the preceding winter months.

Figure 7

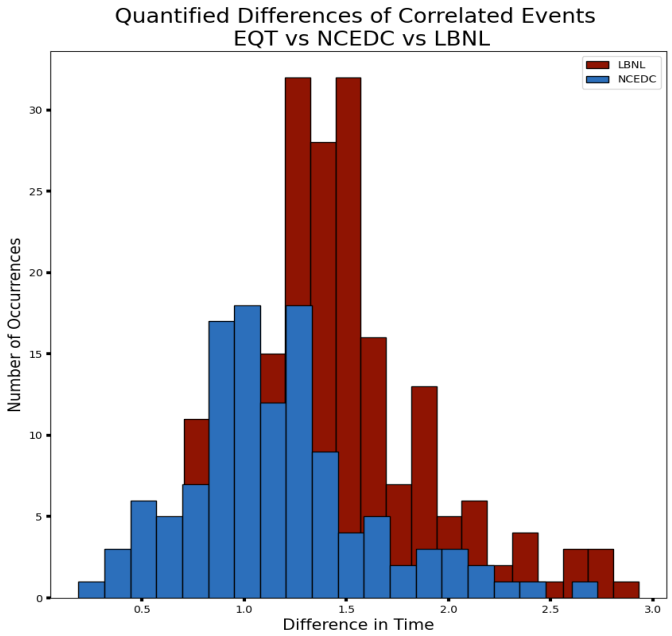

Histogram showing distribution of differences between EQT & NCEDC picks (blue), EQT & LBNL picks (red). The values are absolute differences, as pick strategies are not necessarily consistent between events or catalog. Average difference is 1.0 seconds for NCEDC and 1.4 seconds for LBNL. The events display a distribution similar to a Gaussian or Poisson distribution, although no formal distribution testing was performed.

5 Discussion

5.1 Findings & Synthesis

Both the LBNL and NCEDC catalogs accurately characterize the seismic nature of The Geysers, but the LBNL catalog has statistical robustness not found in the NCEDC catalog due to a difference in size. However, it is clear from spatial analysis that at least part of the LBNL event identification system is automated or uses incremental methods to assign values, and it is unclear if, and to what degree, the catalog is parsed. By contrast, the NCEDC catalog appears to use less organized methods with respect to time and space. It is possible that the NCEDC catalog has been parsed for events that could otherwise be matched between catalogs. In spite of this speculation, the low sensor density within the study area relative to the LBNL network, and the comparatively lower sampling rate and sensitivity suggest the difference between the catalogs is simply due to array precision.

The Geysers area is characterized by near-constant, low intensity seismic events, with an average intensity of approximately 1 M_L or M_d. Seismicity in the field area is localized to anthropogenic sources, in particular effluent-injection wells. The field's northern region is characterized by deeper (2 to > 4 km), more intense seismic activity (> avg intensity), and displays depth-oriented features that are loosely correlated to injection well sites. The southern area exhibits very shallow seismic activity that is nonetheless organized around injection wells; however, this region shows lower correlation with injection wells in map-view. The geothermal field as a whole displays seismic activity rates proportional to volume of effluent injection with a delay of 2-4 months, as described by Johnson et al. (2016). Due to the rate of seismic activity and lack of clear epicenter or hypocenter localizing-features, it appears that more advanced methods are needed to properly resolve seismicity correlation with well sites, relation to structural features, and detailed rates of seismic activity relative to anthropogenic events.

Both the NCEDC and LBNL catalogs were verified using independent catalog development to an average resolution of 1 to 1.5 seconds, respectively. The catalogs correlated 99% of events between our EQT-generated catalog and the respective catalog. Our location-estimation method failed, likely due to the lack of sophistication; this is seen as credit to the catalogs, instead. Indeed, between the two catalogs cross-sectional analysis in time displayed temporally-parallel events with nearly identical geospatial coordinates, indicating high correlation between provider catalog events. However, a variety of differences suggests the events in one catalog are not dependent upon another.

5.2 Conclusions

The geophysical characteristics of The Geysers are incredibly complicated on account of the existing tectonic & geologic background, which are complicated even further by nearly 80 years of geothermal exploitation. The statistical and analytic methods used in this analysis were comparatively simple, but nonetheless

provided strong evidence for the quality and relation of events in the catalogs. Further refinement of these methods would include sampling longitudes and latitude over narrow bands to produce image slices akin to an MRI, modification of the maximum-likelihood estimation (e.g. Bender, 1983), and application of more sophisticated location estimation methods around injection well sites. Nevertheless, we were able to validate two catalogs and distinguish characteristic phenomenon identified by previous research in the field area.

Citations

Aki, K. (1965). Maximum likelihood estimate of b in the formula log N= a-bM and its confidence limits. *Bull. Earthq. Res. Inst., Tokyo Univ*, *43*, 237–239.

Bender, B. (1983). Maximum likelihood estimation of b values for magnitude grouped data. *Bulletin of the Seismological Society of America*, *73*(3), 831–851. https://doi.org/10.1785/bssa0730030831

Boyle, K., & Zoback, M. (2014). The stress state of the northwest geysers, california geothermal field, and implications for Fault-Controlled fluid flow. *Bulletin of the Seismological Society of America*, *104*(5), 2303–2312. https://doi.org/10.1785/0120130284

Dalrymple, G., Grove, M., Lovera, O. M., Harrison, T., Hulen, J. B., & Lanphere, M. A. (1999). Age and thermal history of the geysers plutonic complex (felsite unit), geysers geothermal field, california: A 40Ar/39Ar and U–Pb study. *Earth and Planetary Science Letters*, *173*(3), 285–298. https://doi.org/10.1016/s0012-821x(99)00223-x

Donnelly, J. M., Hearn, B. C., & Goff, F. E. (1977). *The Clear Lake volcanics, California: Geology and field trip guide*. Geological Society of America. https://www.geothermal-library.org/index.php?mode=pubs&action=view&record=1019357

El-Isa, Z., & Eaton, D. W. (2014). Spatiotemporal variations in the b-value of earthquake magnitude–frequency distributions: Classification and causes. *Tectonophysics*, *615–616*, 1–11. https://doi.org/10.1016/j.tecto.2013.12.001

Guilhem, A., Hutchings, L., Dreger, D. S., & Johnson, L. R. (2014). Moment tensor inversions of m ~ 3 earthquakes in the geysers geothermal fields, california. *Journal of Geophysical Research: Solid Earth*, *119*(3), 2121–2137. https://doi.org/10.1002/2013jb010271

Hearn, B. C., Donnelly-Nolan, J. M., & Goff, F. E. (1995). *Geologic map and structure sections of the clear lake volcanics, northern california* [Map]. USGS Public Warehouse. http://pubs.usgs.gov/imap/2362/

Hearn, C., Donnelly-Nolan, J. M., & Goff, F. E. (1981). The Clear Lake volcanics: Tectonic setting & magma sources. *USGS Professional Report 1411*, 25–45.

Hulen, J. B., & Nielson, D. L. (1996). The geysers felsite. *Geothermal Resources Council Transactions*, *20*.

Hutchings, L., Bonner, B., Singh, A., & Jarpe, S. (2014). Micro-earthquake analysis for reservoir properties at the prati-32 injection test, the geysers, california. *Proceeding, Geothermal Resources Council, August*.

Johnson, C. M., & O'Neil, J. R. (1984). Triple junction magmatism: A geochemical study of neogene volcanic rocks in western california. *Earth and Planetary Science Letters*, *71*(2), 241–262. https://doi.org/10.1016/0012-821x(84)90090-6

Johnson, C. W., Totten, E. J., & Bürgmann, R. (2016). Depth migration of seasonally induced seismicity at The Geysers geothermal field. *Geophysical Research Letters*, *43*(12), 6196–6204. https://doi.org/10.1002/2016gl069546

Leptokaropoulos, K. (2020). Magnitude distribution complexity and variation at the geysers geothermal field. *Geophysical Journal International*, *222*(2), 893–906. https://doi.org/10.1093/gji/ggaa208

Leptokaropoulos, K., Staszek, M., Lasocki, S., Martínez-Garzón, P., & Kwiatek, G. (2017). Evolution of seismicity in relation to fluid injection in the North-Western part of the geysers geothermal field. *Geophysical Journal International*, *212*(2), 1157–1166. https://doi.org/10.1093/gji/ggx481

Majer, E. L., Baria, R., Stark, M., Oates, S., Bommer, J., Smith, B., & Asanuma, H. (2007). Induced seismicity associated with enhanced geothermal systems. *Geothermics*, *36*(3), 185–222. https://doi.org/10.1016/j.geothermics.2007.03.003

McLaughlin, R. J. (1981). Tectonic setting of pre-Tertiary rocks and its relation to geothermal resources in the Geysers-Clear lake area. *US Geol. Surv. Prof. Pap*, *1411*, 3–23.

McLaughlin, R. J., & Ohlin, H. N. (1984). Tectonostratigraphic framework of the Geysers-Clear lake region, california. *Franciscan Geology of Northern California*, 221–254.

Mousavi, S. M., Ellsworth, W. L., Zhu, W., Chuang, L. Y., & Beroza, G. C. (2020). Earthquake transformer—an attentive deep-learning model for simultaneous earthquake detection and phase picking. *Nature Communications*, *11*(1). https://doi.org/10.1038/s41467-020-17591-w

Peacock, J. R., Earney, T. E., Mangan, M. T., Schermerhorn, W. D., Glen, J. M., Walters, M., & Hartline, C. (2020). Geophysical characterization of the northwest geysers geothermal field, california. *Journal of Volcanology and Geothermal Research*, *399*, 106882. https://doi.org/10.1016/j.jvolgeores.2020.106882

Schmitt, A. K., Grove, M., Harrison, T., Lovera, O., Hulen, J., & Walters, M. (2003a). The geysers - cobb mountain magma system, california (part 1): U-Pb zircon ages of volcanic rocks, conditions of zircon crystallization and magma residence times. *Geochimica et Cosmochimica Acta*, *67*(18), 3423–3442. https://doi.org/10.1016/s0016-7037(03)00140-6

Schmitt, A. K., Grove, M., Harrison, T., Lovera, O., Hulen, J., & Walters, M. (2003b). The Geysers-Cobb mountain magma system, california (part 2): Timescales of pluton emplacement and implications for its thermal history. *Geochimica et Cosmochimica Acta*, *67*(18), 3443–3458. https://doi.org/10.1016/s0016-7037(03)00126-1

Thurber, C. H. (1983). Earthquake locations and three-dimensional crustal structure in the Coyote Lake Area, central California. *Journal of Geophysical Research*, *88*(B10), 8226. https://doi.org/10.1029/jb088ib10p08226

Wiemer, S., & Wyss, M. (2000). Minimum Magnitude of Completeness in Earthquake Catalogs: Examples from Alaska, the Western United States, and Japan. *Bulletin of the Seismological Society of America*, *90*(4), 859–869. https://doi.org/10.1785/0119990114

Yu, C., Vavryčuk, V., Adamová, P., & Bohnhoff, M. (2018). Moment tensors of induced microearthquakes in the geysers geothermal reservoir from broadband seismic recordings: Implications for faulting regime, stress tensor, and fluid pressure. Journal of Geophysical Research: Solid Earth, 123(10), 8748–8766. https://doi.org/10.1029/2018jb016251